Applied Surface Science 600 (2022) 153947

Contents lists available at ScienceDirect

Applied Surface Science

journal homepage: www.elsevier.com/locate/apsusc

Full length article

# Adsorption and decomposition of ZDDP on lightweight metallic substrates: Ab initio and experimental insights

Stefan Peeters [a], Alberto Barlini [b], Jayant Jain [c], Nitya Nand Gosvami [c], M.C. Righi [a,d,*]

[a] Department of Physics and Astronomy, University of Bologna, Viale Carlo Berti Pichat 6/2, Bologna, 40127, Italy
[b] Department of Chemical, Pharmaceutical and Agricultural Sciences, University of Ferrara, Via Luigi Borsari 46, Ferrara, 44121, Italy
[c] Department of Materials Science and Engineering, Indian Institute of Technology Delhi, Hauz Khas, New Delhi, 110016, India
[d] Department of Mechanical Engineering, Imperial College London, South Kensington Campus, London SW7 2AZ, UK

ARTICLE INFO

*Keywords:*
Interfaces
ZDDP
Tribochemistry
Ab initio simulations
AFM
Friction
Lubricants
Automotive applications
Lightweight alloys

ABSTRACT

Lightweight alloys substitute steel in a wide range of industrial applications. It is still unclear whether the lubricant additives currently employed to reduce friction of sliding metallic parts are also efficient on non-ferrous substrates. In particular, the functionality of zinc dialkyldithiophosphates (ZDDPs) in contact with Al- and Mg-containing alloys still needs to be understood. In this work, we describe the properties of ZDDP at Al(111), Al(001), Al(331), Mg(0001) and $Mg_{17}Al_{12}$ surfaces and interfaces. Our calculations indicate that molecular fragments originated from ZDDP chemisorb more strongly on the intermetallic phase $Mg_{17}Al_{12}$ with respect to aluminum and magnesium, due to the higher surface energy of the mixed substrate. Ab initio molecular dynamics simulations show that the kinetics of the additive decomposition is significantly different on Al and the mixed phase. These results are supported by atomic force microscopy sliding tests, which revealed that the tribofilm formation is observed only on the latter substrate. This work suggests that the tribological performance of lightweight alloys can be enhanced by increasing the additive-surface chemical interactions.

## 1. Introduction

Friction is a common phenomenon which results in massive energy and environmental costs. Holmberg and Erdemir estimated that approximately 21% of the total energy extracted from fuel in a passenger car is needed to move the vehicle, while the rest is lost and one third of this energy loss is due to friction [1,2]. One way to reduce energy losses between sliding metallic parts in several industrial applications is by introducing friction modifier additives in the lubricating oil. In particular, extreme pressure (EP) additives react in severe tribological conditions to form chemical species able to protect the surfaces, offering low resistance to sliding. Zinc dialkyldithiophosphates (ZDDPs) are among the most successful EP additives due to their remarkable antiwear properties [3–5], especially on steel [6–8]. The decomposition of ZDDP can occur spontaneously in lubricant mixtures at elevated temperatures, leading to the formation of thermal films, and also in the presence of mechanical stresses, which produce tribofilms at lower temperatures compared to the ones required for the thermal films. Tribofilms are composed of layered pads and are generally more wear-resistant compared to thermal films [9], which are rather continuous, yet their composition is similar. The topmost layer is an adsorption layer of ZDDP and other sulfur-containing molecules, while the inner layers are composed of polyphosphates chains that are longer at the top of the pads and shorter at the bottom [3]. Iron particles generated by wear can be included in the bottom layer of the tribofilm [6], changing the color of the tribofilm from blue to brown [10]. For this reason, ZDDP is also considered as an efficient antioxidant and anti-corrosive agent. Furthermore, the antiwear properties of ZDDP can be enhanced by laser patterning the surfaces hosting the tribofilm [11].

Lightweight materials are becoming extremely important for energy savings in many applications [12], especially in the automotive industry, where aluminum and magnesium alloys substitute steel to reduce fuel consumption [13]. Indeed, research concerning ZDDP recently shifted towards understanding its interaction with non-ferrous substrates. Ueda et al. studied the formation of ZDDP-based tribofilms on different non-ferrous substrates and found out that the tribofilms are either very difficult to form or easily removable in boundary lubrication conditions [14]. Wan et al. demonstrated that ZDDP forms thin tribofilms which are not sufficient to prevent wear on A2024 aluminum alloys [15]. The chemical composition of such tribofilms has also been investigated on the Al- and Si-containing A383 alloy and it turned out that the lengths of the polyphosphate chains depend on the temperature and on the chemical nature of the substrate [16].

* Corresponding author.
*E-mail address:* clelia.righi@unibo.it (M.C. Righi).

https://doi.org/10.1016/j.apsusc.2022.153947
Received 11 April 2022; Received in revised form 26 May 2022; Accepted 10 June 2022
Available online 17 June 2022

Recently, in-situ experiments by Gosvami et al. indicated the formation of ZDDP-derived tribofilms on ADC12, an Al–Si alloy, under lubricated conditions [17]. The tribofilms formed on the regions containing Si are thicker, smoother and provide lower friction coefficients than the Al matrix. Another study showed that thin tribofilms only form on top of a mixed $Mg_{17}Al_{12}$ phase, while they were not observed on the $\alpha$-Mg matrix [18]. However, these studies could not fully explain the reason why the substrate composition is so crucial for enabling the tribofilm formation. Several authors suggested that the hardness of the substrates could be a key factor in determining the quality of the tribofilm [8,18,19], although the chemistry of the surface may also play a substantial role.

Computer simulations offer a valuable perspective on the mechanism of formation of the tribofilms on metallic substrates, by effectively describing chemical interactions at the atomic level [20–24]. Martin et al. investigated ZDDP on ferrous surfaces by molecular dynamics [25]. They extended their investigation to the digestion of silica and alumina nanoparticles in the zinc phosphate by using a hybrid computational technique based on the tight-binding approximation [26]. However, to the best of our knowledge, no systematic study has been performed yet concerning the interfaces of these lightweight alloys. Here, we present a detailed investigation based on density functional theory (DFT), including ab initio molecular dynamics simulations, and atomic force microscopy sliding experiments to shed light on the interaction of ZDDP with aluminum, magnesium and $Mg_{17}Al_{12}$ surfaces and interfaces. First principles calculations are essential to properly describe the chemical interaction between the additive and the substrates. These techniques have not been used to explore the reactivity of lightweight alloys yet. Our aim is to describe how ZDDP and its fragments adsorb on these materials to better understand the initial steps of the tribofilm formation and gain insights into the mechanism behind the lubrication of lightweight alloys.

## 2. Systems and methods

### 2.1. Computational methods

We performed density functional theory calculations following the plane waves and pseudopotentials approach implemented in Quantum ESPRESSO [27]. The kinetic energy cutoff for the wave functions and charge densities were 40 and 320 Ry, respectively. The Perdew, Burke and Ernzerhof (PBE) [28] approximation was used for the exchange–correlation functional. The pseudopotentials used to represent the electronic configuration of the atoms were Ultrasoft, following the GBRV parametrization [29] for Mg and the RRKJ parametrization [30] for all the other atoms. Spin polarization was considered to avoid the restriction of the electronic configuration to a closed shell. Periodic boundary conditions were used in all the calculations. A Gaussian smearing was added to better describe electronic occupations around the Fermi level. The width of the Gaussian functions was 0.001 Ry. The geometries of the systems were optimized using the BFGS algorithm [31] and the optimizations were stopped when the total energy and the forces converged under the thresholds of $10^{-4}$ Ry and $10^{-3}$ Ry/bohr, respectively.

The chemical structure of ZDDP consists of a zinc atom coordinated by two dialkyldithiophosphate anions. In our calculations, the lateral alkyl chains of the ZDDP molecule were reduced to methyl groups to minimize the computational cost. We justified this choice in a previous work concerning MoDTC additives, where we showed that the dissociation energies of methyl groups and longer alkyl chains in the ligand units are similar [23]. Since the lateral alkyl chains are connected to electronegative atoms in both compounds, i.e. $N$ and O atoms in MoDTC and ZDDP, respectively, we believe that reducing the lateral chains to methyl groups may be reasonable also for ZDDP. Indeed, the alkyl chains are not part of the inner tribofilm [3,6] and should be dissolved in the lubricant oil after the decomposition. The chemical structure of ZDDP was initially generated with the Avogadro molecular builder and visualization tool [32] and then optimized in a cubic supercell with an edge of 30 Å. The final geometry of ZDDP is shown in Fig. 1a.

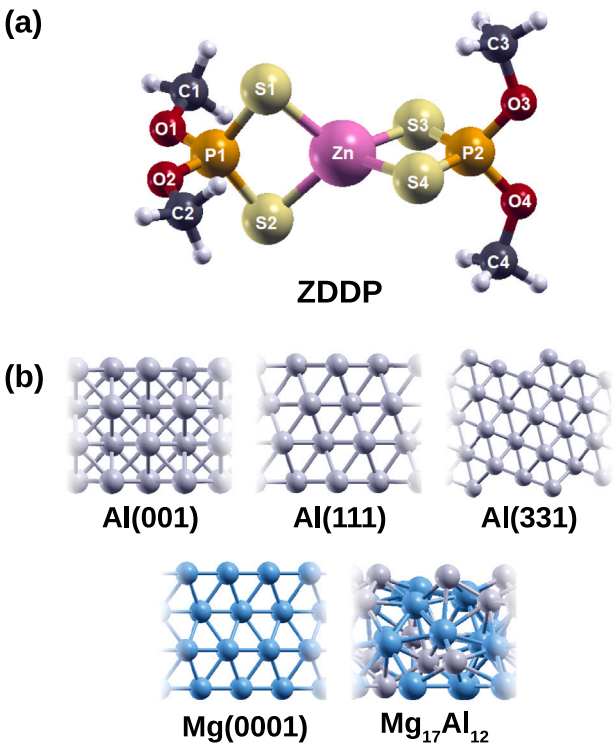


**Fig. 1.** (a) Optimized geometry of the ZDDP molecule. (b) Lateral views of the metallic substrates considered in this study.

Fig. 1b shows the metallic substrates considered in this work, namely Al(111), Al(001), Al(331), Mg(0001) and a mixed $Mg_{17}Al_{12}$ phase. These surfaces are representative models for the substrates considered in the experiments. The lattice parameters of bulk Al and Mg turned out to be $a_{Al} = 4.046$ Å, $a_{Mg} = b_{Mg} = 3.1928$ Å, $c_{Mg} = 5.1939$ Å. A 16 × 16 × 16 Monkhorst-Pack grid was used to sample the reciprocal space for the bulk structure of Al. The K-points sampling was properly rescaled for all the subsequent simulations. The convergence tests performed on the systems aimed at an accuracy of 2 meV/atom on the total energy, as explained in detail in the Supporting Information. Finally, the lattice parameters of the $Mg_{17}Al_{12}$ structure were optimized by a variable-cell calculation, with the initial geometry obtained from the Materials Project database [33]. The lattice parameter and the angles of the $Mg_{17}Al_{12}$ cell turned out to be 9.1215 Å, $\alpha = \gamma = 70.5°$ and $\beta = 109.5°$. The Al(111), Al(001) and Mg(0001) slabs used to adsorb the ZDDP molecule were composed of 4 atomic layers, and their lateral dimensions were 3 × 3, 4 × 3 and 6 × 3, respectively. The Al(331) slab, generated from the geometry available on the Materials Project database [33], was composed by 12 atomic layers and was replicated 6 times along the $x$ and 2 times along the $y$ directions. The optimized structure of $Mg_{17}Al_{12}$ was simply replicated two times along the $x$ direction.

The surface energies of the substrates were calculated as follows:

$$E_{surface} = \frac{E_{slab} - n \cdot E_{bulk}}{2A} \quad (1)$$

where $E_{slab}$, $E_{bulk}$ are the total energies of the slabs and of the bulk structures, respectively, $n$ is the ratio between the number of atoms in the slab and in the bulk, and A is the area of the simulation cell. $E_{slab}$ was calculated using a K-point sampling equivalent to the one used for $E_{bulk}$.

The adsorption energies of the ZDDP additive on the substrates were calculated as:

$$E_{ads} = E_{mol+sub} - E_{mol} - E_{sub} \quad (2)$$

where $E_{mol+sub}$, $E_{mol}$ and $E_{sub}$ are the total energies of the whole adsorbed system, the isolated ZDDP molecule and the substrate alone, respectively.

To investigate the behavior of ZDDP under mechanical stresses, the geometry of the molecule at the metallic interfaces was also optimized. Vertical forces, corresponding to a load of 1 GPa, were imposed on the external atoms of the top metallic slab, while the external atoms of the bottom slab were kept fixed.

Born–Oppenheimer Molecular Dynamics simulations were performed starting from the compressed interfaces of Al(111) and $Mg_{17}Al_{12}$. The integration of the charge density was carried out only at the $\Gamma$-point, and a time step of approximately 0.97 fs was used. The temperature was fixed at 380 K. The sliding motion was simulated by an ad hoc modified version of the program [34,35].

Several pictures in this work were realized using the XCrySDen software [36].

### 2.2. Experimental methods

Commercially available as-cast AZ91 (Mg–9Al–1Zn, wt.%) Mg alloy (Alfa Aesar, Ward Hill, MA, USA) was wire cut into 30 mm × 30 mm × 2.5 mm blocks. The samples were polished using 500 to 4000 grit emery paper followed by polishing in a colloidal silica medium of size 0.05 μm. The samples were subsequently etched in 10% Nital solution for microstructural examination. After polishing, the final roughness of the alloy was measured using AFM imaging in contact mode and the RMS roughness values for the $Mg_{17}Al_{12}$ precipitate and the Mg matrix were 1.45 nm and 1.56 nm, respectively. Finally, the samples were ultrasonicated in acetone for 15 min and then dried under a jet of nitrogen to avoid the contamination for further experimental examination.

Specimen of commercially available ADC12 alloy (composition: 0.30% Mg, 0.78% Fe, 0.22% Mn, 0.81% Cu, 0.70% Zn, 11.3% Si, from Ye Chiu Non-Ferrous Metals, Johor, Malaysia) were machined and cut by electro-discharge machining (EDM) to the size of 30 mm × 30 mm × 2.5 mm for the AFM experiments. After cutting, the samples were polished using SiC papers of various grit sizes ranging from 240–1200, and then final polishing was performed using 6 μm diamond paste followed by 1 μm diamond paste on a napped cloth. Finally, additional polishing was performed by using 1 μm colloidal alumina suspension, followed by 0.05 μm colloidal silica suspension as the final polishing medium. RMS roughness of 3.61 and 5.37 nm was observed for the Si precipitate and the Al matrix, respectively. The sample cleaning was performed by ultrasonication with acetone followed by ethanol, each for about 15–20 min and then immediately drying the sample under a stream of nitrogen gas.

A group II base oil (MAK 65, BPCL, India, viscosity of 11–12.2 cst at 40 °C and 3 cst at 100 °C), mixed with 1 wt% secondary ZDDP (C-TEC 209, Tianhe, China, 8.0–11.0 cst at 100 °C), was used for in situ liquid mode experiments. AFM was used to monitor the growth of the tribofilm and the friction force simultaneously as a function of sliding time. Commercially available silicon cantilevers (Tap190ALG, Budget sensors, Bulgaria), which were further modified by attaching a wear-resistant alumina microsphere of diameter 20-30 μm near the end of the cantilever, were used to measure the topographic evolution within the sliding zone. Contact diameter and contact pressures in different regions were calculated using the Hertzian contact model [37], assuming a Young's modulus of 70 and 80 GPa for Al and $Mg_{17}Al_{12}$ precipitates, respectively The liquid cell, made of polyether ether ketone (PEEK), with the Viton O-ring was mounted over the sample, placed on a heating stage, and was filled with ZDDP-containing base oil. All experiments were performed at 110 °C to observe the tribofilm growth. This temperature was chosen to compare the results with previous ZDDP tribofilm growth experiments conducted at nanoscale as well as macroscale [3,8,37]. Indeed, tribofilm growth does not occur at room temperature. The AFM scan size was 12 μm × 5 μm, and sliding speed was fixed to 80 ms per line scan, which corresponds to a sliding velocity of 150 μm/s. Sliding tests were performed for almost 2 h to observe the tribofilm formation on the surface of the alloys.

## 3. Results and discussion

### 3.1. Bond strength in the ZDDP molecule

The first step of our investigation was the geometry optimization of the ZDDP chemical structure and the calculation of its fragmentation energies. Several studies have already described the geometry of isolated ZDDP [38–40]. We reported the structural data of ZDDP in the Supporting Information, and the bond lengths and angles are in good agreement with the data available in the literature. Furthermore, we evaluated possible fragmentation patterns of the molecule to estimate which bonds will be broken first in tribological conditions, in analogy with our previous studies [23,41,42]. The different fragmentation patterns are schematically represented in Fig. 2.

Cut 1 refers to the breaking of two Zn–S bonds on the same side of the additive, Cut 2 represents the breaking of the Zn–S and P–S bonds, while Cut 3 corresponds to the dissociation of the P–S bonds. Cut 4 and Cut 5 reproduce the formation of methyl and methoxy groups, respectively. All the molecular fragments were considered as radicals, effectively making these fragmentation patterns homolytic bond ruptures. This approach is meant to qualitatively estimate the strength of the different bonds. The calculated fragmentation energies reported in Fig. 2 suggest that Cut 1 is the most favorable fragmentation pattern for isolated ZDDP, as less energy is required to separate the two molecular fragments. Indeed, fragments in which the P atom is highly coordinated are more energetically favorable.

### 3.2. Surface energies of the substrates

To better understand the functionality of ZDDP on lightweight alloys, we selected five different substrates: Al(111), Al(001), Al(331), Mg(0001) and $Mg_{17}Al_{12}$. While the (111) and the (0001) surfaces are the most stable surfaces for Al and Mg, respectively, we also considered two surfaces of Al with a similar reactivity, (001) and (331), where the latter also presents surface steps. Finally, $Mg_{17}Al_{12}$ constitutes one of the most widely used Mg-containing alloys, the AZ91 alloy [18]. The values of $E_{surface}$ turned out to be 0.84, 0.96, 0.96, 0.55 and 1.60 J/m$^2$ for Al(111), Al(001), Al(331) and $Mg_{17}Al_{12}$, respectively, indicating that the most reactive surface is the mixed phase. The surface energies are generally in good agreement with the values obtained in our previous high-throughput evaluation [43].

### 3.3. Adsorption of ZDDP on the substrates

Fig. 3 shows the optimized geometries of the complex adsorbed on the different substrates.

These simulations indicate that ZDDP only physisorbs on aluminum, magnesium and the mixed phase. This result is different for ferrous substrates, onto which ZDDP is able to chemisorb and thermally decompose [3,44]. On the lightweight substrates, repulsion between ZDDP and the surface at short distance prevents chemisorption, with the molecule always laying around 3 Å above the surface atoms. The origin of this repulsion could be the methyl groups of the additive, because Al(001) and Al(331) have practically identical surface energies, yet the adsorption energy of ZDDP on Al(331) is almost double with respect to Al(001). Indeed, on Al(331), the sulfur atoms of ZDDP point directly to the Al atoms of the steps, while the methyl groups have more room, as shown in the *xz* view of the Al(331) surface in Fig. 3.

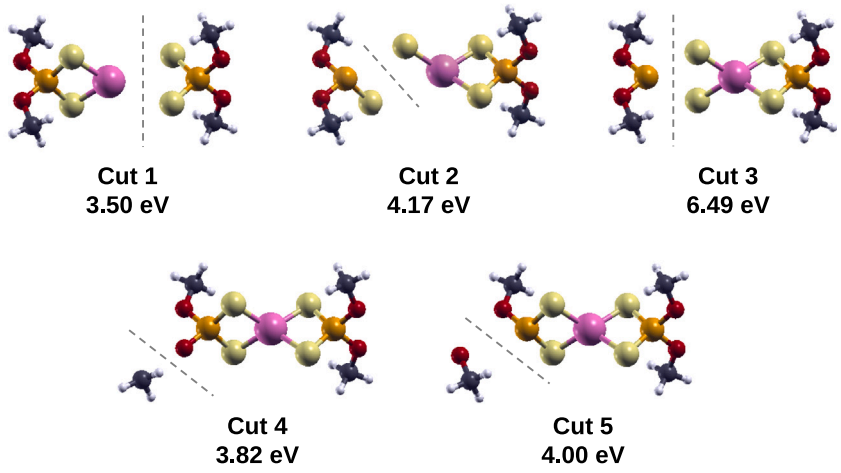


**Fig. 2.** Fragmentation patterns of ZDDP considered in this work, along with the corresponding fragmentation energies.

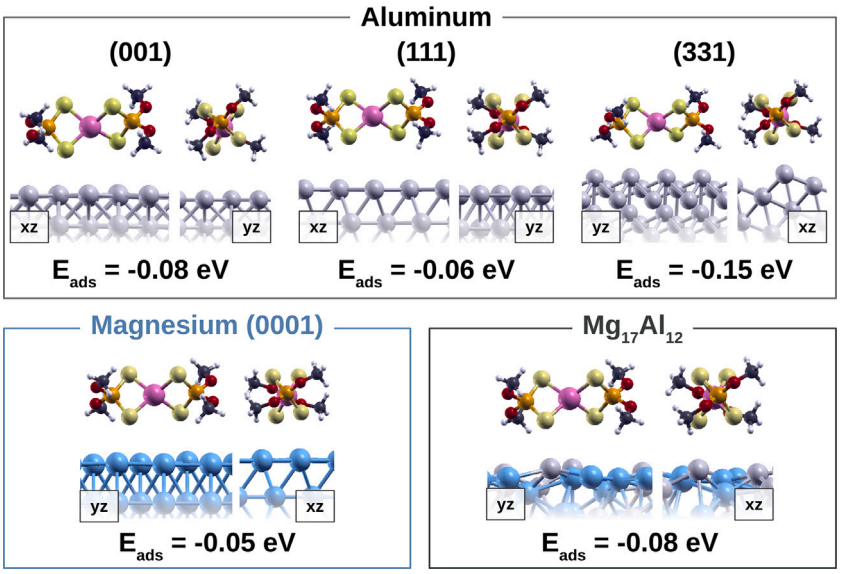


**Fig. 3.** Optimal geometries of the ZDDP additive physisorbed on the different surfaces, along with the respective adsorption energies. For each system, the lateral views from both the *xz* and *yz* orientations are shown.

In all the systems, the interaction among periodic replicas of the ZDDP molecules was found below 0.02 eV. We estimated that ZDDP occupies approximately 60 Å$^2$ on the different surfaces, leading to a surface coverage in the range 30%–47%.

### 3.4. ZDDP at the interfaces under load

The low reactivity of the Al and Mg substrates was observed even when ZDDP was at the metallic interface. In all these simulations, the molecules experienced 1 GPa of load, generated by imposing vertical forces on the external atoms of the slabs. Fig. 4 shows the final geometries of these systems.

The presence of an applied load typically increases the rate of molecular dissociation [34]. Despite the high pressure applied on the system, no significant changes in the chemical structure of the ZDDP molecule were observed on aluminum and magnesium. Indeed, the molecule overall maintained its geometry and did not strongly interact with the surfaces. On the other hand, the ZDDP molecule dissociated at the $Mg_{17}Al_{12}$ interface. The Zn atom partially lost the coordination by the S atoms and interacted with the Al and Mg atoms of the bottom surface. A $(CH_3O)_2PS_2$ unit was detached from the molecule, corresponding to one of the fragments originated by Cut 1, i.e. the most favorable fragmentation pattern, as predicted by the calculations for the isolated molecule. The different behavior of ZDDP under load demonstrated that the $Mg_{17}Al_{12}$ phase is more reactive than the pristine elements. In addition, we calculated the energy change upon formation of a compressed interface from the separated surface and countersurface:

$$\Delta E = E_{interface} - E_{mol+sub} - E_{sub} \quad (3)$$

where $E_{interface}$ is the total energy of the system under load. Positive (negative) values of $\Delta E$ indicate that the compressed system is less (more) favorable than the situation of the physisorbed molecule without any load, with the top slab at infinite distance from ZDDP. As it can be seen from the results reported in Fig. 4, the only negative value was observed for the $Mg_{17}Al_{12}$ interface.

### 3.5. Adsorption of molecular fragments of ZDDP on the substrates

To shed light on the results concerning the interfaces under load, we considered the adsorption of fragments of ZDDP on the Al(111), Mg(0001) and $Mg_{17}Al_{12}$ surfaces. Comparing the adsorption energies

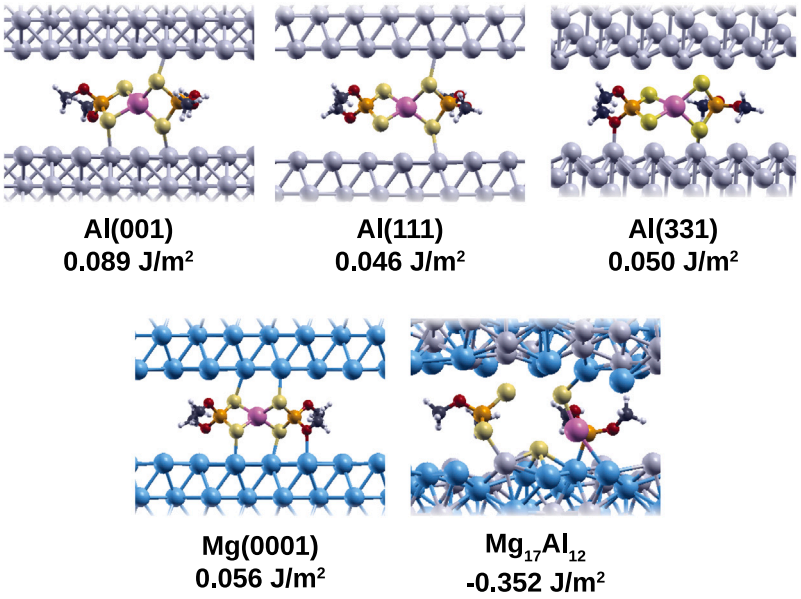


**Fig. 4.** Optimized geometries of the ZDDP molecule at the interface of the different metallic substrates, experiencing 1 GPa of load. The values of $\Delta E$ are reported below each system.

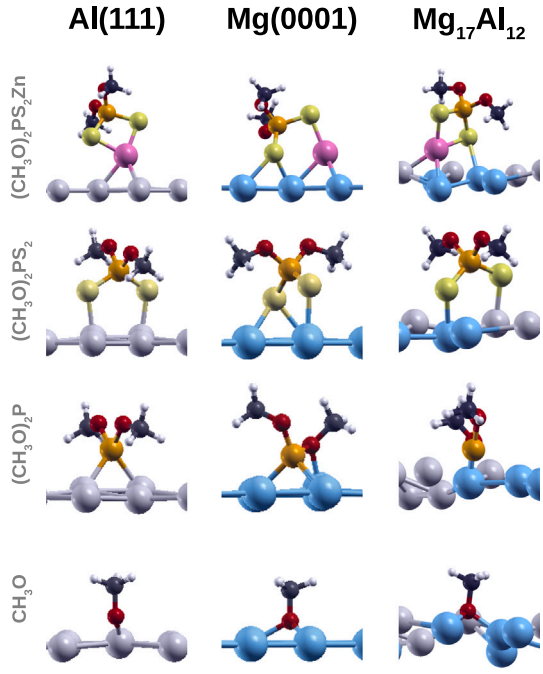


**Fig. 5.** Fragments of ZDDP adsorbed on Al(111), Mg(0001) and $Mg_{17}Al_{12}$. For each system, the lateral view is shown. For the top views, the reader is referred to the Supporting Information. Only the highest atomic layer of the slabs is shown in the pictures.

of these fragments allows to estimate their affinity for the different substrates and gain insights into the dissociation mechanism of the additive. We considered the $(CH_3O)_2PS_2$, the $(CH_3O)_2P$ and the $CH_3O$ units originated from Cuts 1, 3 and 5, respectively. In addition, we also considered the complementary fragment of Cut 1, $(CH_3O)_2PS_2Zn$, which is useful to estimate the dissociation energy of ZDDP on the different substrates. The optimized geometry of these fragments is shown in Fig. 5.

Table 1 reports the adsorption energies of the fragments, as calculated in Eq. (2).

**Table 1**
Adsorption energies obtained for the analyzed ZDDP fragments on the Al (111), Mg (0001) and $Mg_{17}Al_{12}$ surfaces.

| Fragment | $E_{ads}$ (eV) | | |
|---|---|---|---|
| | Al (111) | Mg (0001) | $Mg_{17}Al_{12}$ |
| $(CH_3O)_2PS_2Zn$ | −1.85 | −1.68 | −2.08 |
| $(CH_3O)_2PS_2$ | −2.43 | −2.62 | −2.72 |
| $(CH_3O)_2P$ | −1.26 | −1.56 | −1.66 |
| $CH_3O$ | −3.27 | −3.89 | −3.95 |

The adsorption on the $Mg_{17}Al_{12}$ surface turned out to be more favorable compared to Al(111), as expected from the higher reactivity of this substrate. Moreover, the chemisorption of the fragments on Mg(0001) turns out to be more favorable than on Al(111). This result is in contrast with the fact that the surface energy of Mg(0001) is lower than the one of the more reactive Al(111). The larger (negative) adsorption energies observed for Mg are most probably due to the increased number of chemical bonds formed by the fragments on this metal. The $(CH_3O)_2P$ fragment, originated by Cut 3, is characterized by the weakest adsorption on all the metals. Furthermore, Cut 3 is the most unfavorable pattern for the isolated compound, suggesting that this decomposition pattern is less likely to occur with respect to the other patterns. On the contrary, the release of the methoxy group is favorable, followed by the detachment of the DDP unit.

Finally, we calculated the dissociation energy $E_{diss}$ of ZDDP on the different substrates following Cut 1:

$$E_{diss} = E_{(CH_3O)_2PS_2Zn+sub} + E_{(CH_3O)_2PS_2+sub} - E_{mol+sub} - E_{sub} \quad (4)$$

where $E_{(CH_3O)_2PS_2Zn+sub}$ and $E_{(CH_3O)_2PS_2+sub}$ are the energies of the two fragments chemisorbed on the different substrates. The dissociation energies turned out to be −0.70, −0.75 and −1.22 eV on Al(111), Mg(0001) and $Mg_{17}Al_{12}$, respectively, confirming that the dissociation on the mixed substrate is indeed more energetically favorable.

### 3.6. Born–Oppenheimer Molecular dynamics simulations

To validate the results obtained from the static simulations, we carried out Born–Oppenheimer Molecular Dynamics simulations of the ZDDP molecule at the Al(111) and $Mg_{17}Al_{12}$ interfaces. Al(111) was selected as a representative material for all the other substrates, where

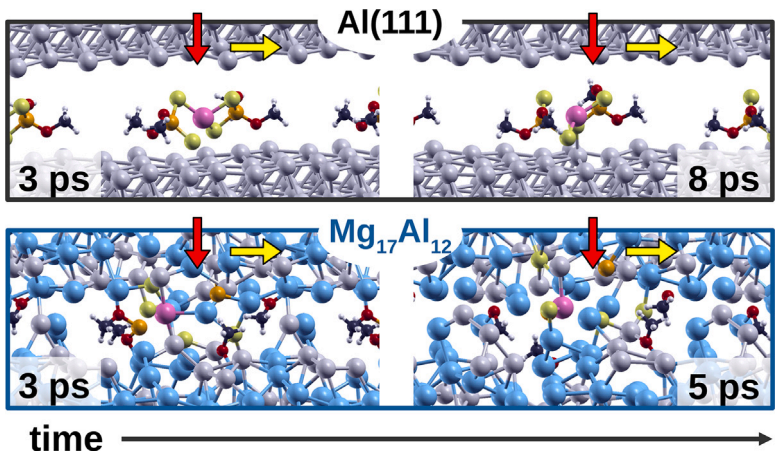


**Fig. 6.** Lateral views of ZDDP at the Al(111) and $Mg_{17}Al_{12}$ interfaces at different times during the dynamic simulations. The red and yellow arrows represent the load of 1 GPa and the sliding motion of 100 m/s, respectively.

a low reactivity of ZDDP was previously observed. Fig. 6 shows the lateral geometries of the systems at different times. Since the initial geometries of the dynamic simulations corresponded to the equilibrium geometries of the interfaces under a load of 1 GPa, shown in Fig. 4, the ZDDP molecule was intact at the beginning of the simulation including Al(111), while the additive was already dissociated in the case of the mixed phase. At the Al(111) interface, the molecule remained undissociated during the whole simulation, lasted 8 ps. The additive mainly interacted with the bottom surface and no decomposition was observed, despite the Zn–S bonds stretching in the range 2.17–2.78 Å. Temperature and sliding on the fragments of ZDDP at the interface of the mixed phase promoted further dissociation. The dithiophosphate units decomposed, releasing the sulfur atoms on the surfaces. At 3 ps, a phosphorus atom was also detached from the methoxy groups. In these conditions, ZDDP could no longer separate the interface. Indeed, the molecule was completely dissociated at 5 ps and the sulfur and phosphorus atoms diffused in the mixed phase. Even though the simulated times were small compared to the duration of the experimental tests, the different behavior of ZDDP at the two interfaces revealed that the kinetics of the tribochemical reaction significantly differs for the two considered substrates.

### 3.7. Discussion

Our simulation demonstrated that ZDDP cannot strongly interact with pure Al and Mg. For these metals, the additive only weakly physisorbs on flat surfaces, while on ferrous materials ZDDP is able to chemisorb and decompose [3,25]. Even the increase of surface reactivity due to the presence of defects, e.g. step edges, is not enough to promote the dissociative chemisorption. This is a challenge for the lightweight metals that are replacing steel in automotive parts. The mixed $Mg_{17}Al_{12}$ turned out to be more efficient than Al and Mg in promoting the decomposition of ZDDP. While the additive physisorbs on the mixed phase, as in the case of the pristine elements, ZDDP is able to decompose under load at the interface of $Mg_{17}Al_{12}$. This phase has a higher surface energy than the surfaces of Al and Mg considered in this work, indicating a higher reactivity of the mixed surface. Furthermore, the calculations suggested that the reactive sites of ZDDP are the sulfur atoms. Fig. 3 indicates that the adsorption of the molecule becomes slightly stronger when the sulfur atoms approach the metallic substrate, as in the case of the Al(331) surface. To further investigate the role of sulfur in the adsorption of ZDDP, we calculated the charge displacement $\rho_{disp}$ arising when ZDDP physisorbs on the Al(111) and the $Mg_{17}Al_{12}$ substrates:

$$\rho_{disp} = \rho_{mol+sub} - \rho_{mol}^{SCF} - \rho_{sub}^{SCF} \quad (5)$$

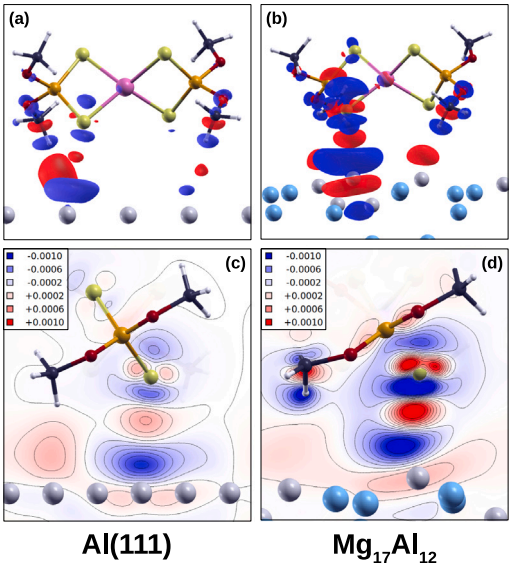


**Fig. 7.** Charge displacement plots of ZDDP adsorbed on Al(111) (left) and $Mg_{17}Al_{12}$ (right). The red and the blue colors of the isosurfaces indicate charge accumulation and depletion, respectively. The size of the atoms was reduced by 50%. (a) and (b) lateral views from the $xz$ plane of the molecule physisorbed on the substrates. The isovalue is 0.0004 electrons per cubic bohr. (c) and (d) lateral views from the $yz$ plane of the physisorbed molecule, with the charge displacement projected on vertical planes passing through the lower sulfur atom. The units for the isovalues in the legends are electrons per cubic bohr.

where $\rho_{mol+sub}$, $\rho_{mol}^{SCF}$ and $\rho_{sub}^{SCF}$ are the charge densities of the adsorbed system, of the molecule and of the substrate alone, at the geometry of the adsorbed system, respectively. The charge displacement, or charge density difference, is an intuitive way to represent the accumulation and the depletion of charge arising from the interaction between the additive and the substrates, and it has been successfully used to demonstrate the connection between the electronic properties and interfacial adhesion [45]. In Fig. 7, the charge displacement plots for the Al(111) and the $Mg_{17}Al_{12}$ substrates are compared. In both cases, a sulfur atom of ZDDP and an interfacing aluminum atom of the substrate lose electronic charge, in favor of the region between them, where a charge accumulation can be observed. In the case of the mixed phase, the charge displacement is visibly larger, as shown by both the 3D (Panels a and b) and the 2D plots (Panels c and d). The charge accumulation between sulfur and aluminum indicates a stronger affinity between them. Indeed, the S–Al distance on Al(111) and $Mg_{17}Al_{12}$ are 3.81

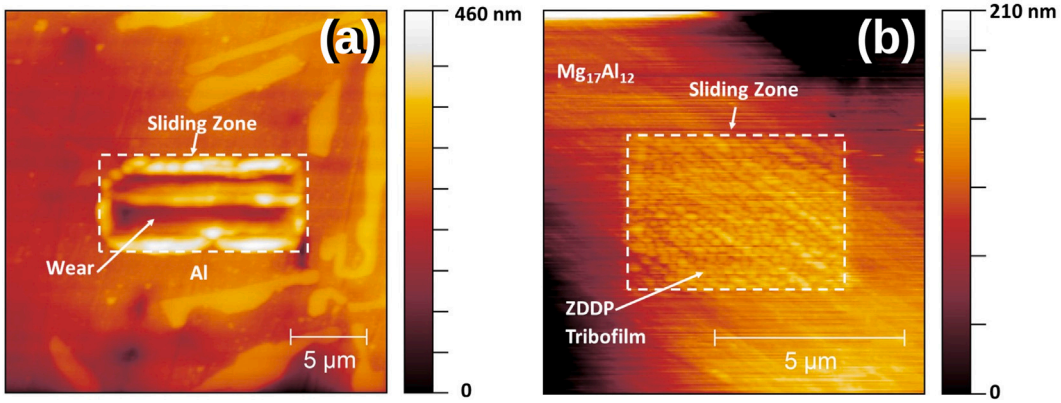


**Fig. 8.** AFM images showing: (a) wear on the Al matrix of the ADC12 alloy, (b) formation of a stable antiwear tribofilm on the $Mg_{17}Al_{12}$ phase of the AZ91 alloy.

and 3.20 Å, respectively. The load of 1 GPa at the $Mg_{17}Al_{12}$ interface is sufficient to reduce the S–Al distance and to overcome the energy barriers associated to the disruption of the S–Zn bond and the formation of the S–Al bond.

It is worth to note that a charge depletion is observed on the hydrogen atoms pointing towards the surface, and a charge accumulation is present below them, suggesting the possibility of a dissociation of the C–H bonds. However, the C–H bond dissociation might be less likely than the one of the S–Zn bond, as we did not observe any significant interaction between H and the substrates in Fig. 4.

These computational results explain the different tribological behavior observed in Fig. 8. In these experiments, an alumina AFM tip slides on top of Al, Mg and $Mg_{17}Al_{12}$ regions of Al- and Mg-based alloys under lubrication of a ZDDP-containing oil. No tribofilm was formed on the Al and Mg regions of the alloys, resulting in significant wear. When tribofilms cannot be formed efficiently, the surfaces remain unprotected and interfacial bonds can arise, generating resistance to the sliding motion. Therefore, significant wear and high friction coefficients can be observed [17]. On the contrary, patches of antiwear tribofilm were formed on $Mg_{17}Al_{12}$. One reason for this different tribological behavior could be the hardness of the intermetallic phase, which is higher than the one the pure elements, as suggested by several authors [18,19]. Sliding on harder materials allows for more energy to be generated at the contact, promoting the reactivity of the additives. However, our simulations under load and the charge displacement analysis clearly indicated that the chemical affinity between ZDDP and the substrates plays a major role in determining the efficiency of the tribofilm formation.

Finally, concerning the decomposition of ZDDP, a DDP unit was detached at the interface of the mixed phase. This decomposition pattern is in agreement with the analysis of the bond strengths in the isolated compound. The detachment of the DDP ligand was already suggested as the first step of the dissociation [46]. However, Mosey et al. did not observe the full detachment of a DDP unit from ZDDP in their Car–Parrinello molecular dynamics simulations [40], while they frequently observed the dissociation of only one S–Zn bond. They also described the formation of alkyl and alkoxy radicals represented here by Cut 4 and 5 and found that the release of alkyl radicals are more favorable than alkoxy radicals when the lateral chains are aliphatic. All these results are in general agreement with the fragmentation energies calculated in this work.

## 4. Conclusions

We investigated the interaction of ZDDP with lightweight metallic substrates by density functional theory simulations and atomic force microscopy experiments. The weakest bonds in ZDDP are those between Zn and S, suggesting that the first dissociation step may occur through the separation of a $(CH_3O)_2PS_2$ unit, i.e. the DDP ligand, from the zinc atom. ZDDP weakly physisorbs on all the substrates considered in this work, namely Al(111), Al(001), Al(331), Mg(0001) and $Mg_{17}Al_{12}$, yet charge displacement plots indicate a significant charge accumulation between the sulfur atoms of ZDDP and the Al atoms of $Mg_{17}Al_{12}$. Indeed, ZDDP decomposes only at the $Mg_{17}Al_{12}$ interface under a load of 1 GPa, and release a DDP unit, in agreement with the prediction for the isolated molecule. The other substrates are not reactive enough to promote the dissociation of the additive. Molecular dynamics simulations at 380 K showed further decomposition of ZDDP at the sliding interface of the mixed phase, while the molecule remains intact at the sliding interface of Al(111) under the same conditions. These results closely match our AFM sliding tests, showing that antiwear tribofilms do not form efficiently on the Al and Mg regions of the intermetallic phase. The tribofilm was observed only on $Mg_{17}Al_{12}$, in agreement with previous studies.

This work demonstrated that the electronic properties of the substrates influence the adhesion properties and the reactivity of ZDDP and provided a possible explanation why ZDDP-based tribofilms can be formed more easily on $Mg_{17}Al_{12}$ than Al. Chemical modifications of the lightweight substrates to promote the formation of additive-surface bonds, especially through the S atoms, might be the key to improve the tribological performance of these substrates.

## CRediT authorship contribution statement

**Stefan Peeters:** Conceptualization, Investigation, Writing – original draft. **Alberto Barlini:** Investigation, Writing – original draft. **Jayant Jain:** Investigation. **Nitya Nand Gosvami:** Conceptualization, Investigation, Supervision, Writing – review & editing. **M.C. Righi:** Conceptualization, Supervision, Funding acquisition, Writing – review & editing.

## Declaration of competing interest

The authors declare the following financial interests/personal relationships which may be considered as potential competing interests: M. Clelia Righi reports financial support was provided by European Research Council.

## Acknowledgments

We are thankful to Edoardo Marquis for the fruitful discussions. These results are part of the “Advancing Solid Interface and Lubricants by First Principles Material Design (SLIDE)” project that has received funding from the European Research Council (ERC) under the European Union’s Horizon 2020 research and innovation program (Grant agreement No. 865633).

## Appendix A. Supplementary data

Supplementary material related to this article can be found online at https://doi.org/10.1016/j.apsusc.2022.153947.

## References


[1] K. Holmberg, A. Erdemir, Influence of tribology on global energy consumption, costs and emissions, Friction 5 (2017) 263–284, http://dx.doi.org/10.1007/s40544-017-0183-5.

[2] K. Holmberg, A. Erdemir, Global impact of friction on energy consumption, economy and environment, FME Trans. 43 (2015) 181–185, http://dx.doi.org/10.5937/fmet1503181H.

[3] H. Spikes, The history and mechanisms of zddp, Tribol. Lett. 17 (2004) 469–489.

[4] A.M. Barnes, K.D. Bartle, V.R. Thibon, A review of zinc dialkyldithiophosphates (zddps): Characterisation and role in the lubricating oil, Tribol. Int. 34 (2001) 389–395.

[5] M.A. Nicholls, T. Do, P.R. Norton, M. Kasrai, G. Bancroft, Review of the lubrication of metallic surfaces by zinc dialkyl-dithiophosphates, Tribol. Int. 38 (2005) 15–39.

[6] J. Martin, Antiwear mechanisms of zinc dithiophosphate: A chemical hardness approach, Tribol. Lett. 6 (1999) 1–8.

[7] A. Neville, A. Morina, T. Haque, M. Voong, Compatibility between tribological surfaces and lubricant additives—how friction and wear reduction can be controlled by surface/lube synergies, Tribol. Int. 40 (2007) 1680–1695, http://dx.doi.org/10.1016/j.triboint.2007.01.019, https://www.sciencedirect.com/science/article/pii/S0301679X07000230. Tribology at the Interface: Proceedings of the 33rd Leeds-Lyon Symposium on Tribology (Leeds, 2006).

[8] N.N. Gosvami, J.A. Bares, F. Mangolini, A.R. Konicek, D.G. Yablon, R.W. Carpick, Mechanisms of antiwear tribofilm growth revealed in situ by single-asperity sliding contacts, Science 348 (2015) 102–106, http://dx.doi.org/10.1126/science.1258788.

[9] G.M. Bancroft, M. Kasrai, M. Fuller, Z. Yin, K. Fyfe, K.H. Tan, Mechanisms of tribochemical film formation: Stabilityof tribo- and thermally-generated zddp films, Tribol. Lett. 3 (1997) 47–51, http://dx.doi.org/10.1023/A:1019179610589.

[10] C. Gachot, C. Hsu, S. Suárez, P. Grützmacher, A. Rosenkranz, A. Stratmann, G. Jacobs, Microstructural and chemical characterization of the tribolayer formation in highly loaded cylindrical roller thrust bearings, Lubricants 4 (2016) http://dx.doi.org/10.3390/lubricants4020019, URL https://www.mdpi.com/2075-4442/4/2/19.

[11] C.-J. Hsu, A. Stratmann, A. Rosenkranz, C. Gachot, Enhanced growth of zddp-based tribofilms on laser-interference patterned cylinder roller bearings, Lubricants 5 (2017) http://dx.doi.org/10.3390/lubricants5040039, URL https://www.mdpi.com/2075-4442/5/4/39.

[12] P. Emadi, B. Andilab, C. Ravindran, Engineering lightweight aluminum and magnesium alloys for a sustainable future, J. Indian Inst. Sci. (2022) http://dx.doi.org/10.1007/s41745-021-00267-9.

[13] M. Tisza, I. Czinege, Comparative study of the application of steels and aluminium in lightweight production of automotive parts, Int. J. Lightweight Mater. Manuf. 1 (2018) 229–238, http://dx.doi.org/10.1016/j.ijlmm.2018.09.001, URL https://www.sciencedirect.com/science/article/pii/S2588840418300301.

[14] M. Ueda, A. Kadiric, H. Spikes, Zddp tribofilm formation on non-ferrous surfaces, Tribol. Online 15 (2020) 318–331, http://dx.doi.org/10.2474/trol.15.318.

[15] Y. Wan, L. Cao, Q. Xue, Friction and wear characteristics of zddp in the sliding of steel against aluminum alloy, Tribol. Int. 30 (1997) 767–772.

[16] G. Pereira, A. Lachenwitzer, M. Kasrai, P. Norton, T. Capehart, T. Perry, Y.-T. Cheng, B. Frazer, P. Gilbert, A multi-technique characterization of zddp antiwear films formed on al (si) alloy (a383) under various conditions, Tribol. Lett. 26 (2007) 103, http://dx.doi.org/10.1007/s11249-006-9125-5, URL https://app.dimensions.ai/details/publication/pub.1017908790.

[17] P. Mittal, Y. Maithani, J. Singh, N. Gosvami, In situ microscale study of tribology and growth of zddp antiwear tribofilms on an al–si alloy, Tribol. Int. 151 (2020) 106419, http://dx.doi.org/10.1016/j.triboint.2020.106419.

[18] D. Kumar, J. Jain, N.N. Gosvami, In situ study of role of microstructure on antiwear tribofilm formation on az91 magnesium alloy under zinc dialkyldithiophosphate containing lubricant, Adv. Energy Mater. 22 (2020) 2000335, http://dx.doi.org/10.1002/adem.202000335, URL https://onlinelibrary.wiley.com/doi/abs/10.1002/adem.202000335.

[19] N.J. Mosey, M.H. Müser, T.K. Woo, Molecular mechanisms for the functionality of lubricant additives, Science 307 (2005) 1612–1615, http://dx.doi.org/10.1126/science.1107895, URL https://www.science.org/doi/abs/10.1126/science.1107895.

[20] A. Vakis, V. Yastrebov, J. Scheibert, L. Nicola, D. Dini, C. Minfray, A. Almqvist, M. Paggi, S. Lee, G. Limbert, J. Molinari, G. Anciaux, R. Aghababaei, S. Echeverri Restrepo, A. Papangelo, A. Cammarata, P. Nicolini, C. Putignano, G. Carbone, S. Stupkiewicz, J. Lengiewicz, G. Costagliola, F. Bosia, R. Guarino, N. Pugno, M. Müser, M. Ciavarella, Modeling and simulation in tribology across scales: An overview, Tribol. Int. 125 (2018) 169–199, http://dx.doi.org/10.1016/j.triboint.2018.02.005, URL https://www.sciencedirect.com/science/article/pii/S0301679X18300756.

[21] M.C. Righi, S. Loehlé, M.I. de Barros Bouchet, D. Philippon, J.M. Martin, Trimethyl-phosphite dissociative adsorption on iron by combined first-principle calculations and xps experiments, RSC Adv. 5 (2015) 101162–101168, http://dx.doi.org/10.1039/C5RA14446A.

[22] M.C. Righi, S. Loehlé, M.I. De Barros Bouchet, S. Mambingo-Doumbe, J.M. Martin, A comparative study on the functionality of s- and p-based lubricant additives by combined first principles and experimental analysis, RSC Adv. 6 (2016) 47753–47760, http://dx.doi.org/10.1039/C6RA07545B.

[23] S. Peeters, P. Restuccia, S. Loehlé, B. Thiebaut, M.C. Righi, Characterization of molybdenum dithiocarbamates by first-principles calculations, J. Phys. Chem. A 123 (2019) 7007–7015, http://dx.doi.org/10.1021/acs.jpca.9b03930.pMID:31318554.

[24] S. Peeters, P. Restuccia, S. Loehlé, B. Thiebaut, M.C. Righi, Tribochemical reactions of modtc lubricant additives with iron by quantum mechanics/molecular mechanics simulations, J. Phys. Chem. C 124 (2020) 13688–13694, http://dx.doi.org/10.1021/acs.jpcc.0c02211.

[25] J.M. Martin, T. Onodera, C. Minfray, F. Dassenoy, A. Miyamoto, The origin of anti-wear chemistry of zddp, Faraday Discuss. 156 (2012) 311–323.

[26] T. Onodera, J.M. Martin, C. Minfray, F. Dassenoy, A. Miyamoto, Antiwear chemistry of zddp: Coupling classical md and tight-binding quantum chemical md methods (tb-qcmd), Tribol. Lett. 50 (2013) 31–39, http://dx.doi.org/10.1007/s11249-012-0063-0.

[27] P. Giannozzi, O. Andreussi, T. Brumme, O. Bunau, M. Buongiorno Nardelli, M. Calandra, R. Car, C. Cavazzoni, D. Ceresoli, M. Cococcioni, et al., Advanced capabilities for materials modelling with quantum espresso, J. Phys.: Condens. Matter 29 (2017) 465901, http://dx.doi.org/10.1088/1361-648x/aa8f79.

[28] J.P. Perdew, M. Ernzerhof, K. Burke, Rationale for mixing exact exchange with density functional approximations, J. Chem. Phys. 105 (1996) 9982–9985.

[29] K.F. Garrity, J.W. Bennett, K.M. Rabe, D. Vanderbilt, Pseudopotentials for high-throughput dft calculations, Comput. Mater. Sci. 81 (2014) 446–452, http://dx.doi.org/10.1016/j.commatsci.2013.08.053, URL https://www.sciencedirect.com/science/article/pii/S0927025613005077.

[30] A.M. Rappe, K.M. Rabe, E. Kaxiras, J.D. Joannopoulos, Optimized pseudopotentials, Phys. Rev. B 41 (1990) 1227–1230, http://dx.doi.org/10.1103/PhysRevB.41.1227, URL https://link.aps.org/doi/10.1103/PhysRevB.41.1227.

[31] D.F. Shanno, Conditioning of quasi-newton methods for function minimization, Math. Comp. 24 (1970) 647–656, URL http://www.jstor.org/stable/2004840.

[32] M. Hanwell, D. Curtis, D.C. Lonie, T. Vandermeersch, E. Zurek, G. Hutchison, Avogadro: An advanced semantic chemical editor, visualization, and analysis platform, J. Cheminform. 4 (2012) 17.

[33] A. Jain, S.P. Ong, G. Hautier, W. Chen, W.D. Richards, S. Dacek, S. Cholia, D. Gunter, D. Skinner, G. Ceder, K. a. Persson, The materials project: A materials genome approach to accelerating materials innovation, APL Maters 1 (2013) 011002, http://dx.doi.org/10.1063/1.4812323, URL http://link.aip.org/link/AMPADS/v1/i1/p011002/s1&Agg=doi.

[34] G. Zilibotti, S. Corni, M.C. Righi, Load-induced confinement activates diamond lubrication by water, Phys. Rev. Lett. 111 (2013) 146101, http://dx.doi.org/10.1103/PhysRevLett.111.146101, URL https://link.aps.org/doi/10.1103/PhysRevLett.111.146101.

[35] S. Loehlé, M.C. Righi, Ab initio molecular dynamics simulation of tribochemical reactions involving phosphorus additives at sliding iron interfaces, Lubricants 6 (2018) http://dx.doi.org/10.3390/lubricants6020031, URL https://www.mdpi.com/2075-4442/6/2/31.

[36] A. Kokalj, Computer graphics and graphical user interfaces as tools in simulations of matter at the atomic scale, Comput. Mater. Sci. 28 (2003) 155–168, http://dx.doi.org/10.1016/S0927-0256(03)00104-6, URL http://www.sciencedirect.com/science/article/pii/S0927025603001046, Proceedings of the Symposium on Software Development for Process and Materials Design.

[37] H. Hertz, Ueber die berührung fester elastischer körper. 1882, 1882, pp. 156–171, http://dx.doi.org/10.1515/crll.1882.92.156.

[38] S. Jiang, R. Frazier, E.S. Yamaguchi, M. Blanco, S. Dasgupta, Y. Zhou, T. Cagin, Y. Tang, W.A. Goddard, The sam model for wear inhibitor performance of dithiophosphates on iron oxide, J. Phys. Chem. B 101 (1997) 7702–7709, http://dx.doi.org/10.1021/jp963835y.

[39] S. Jiang, S. Dasgupta, M. Blanco, R. Frazier, E.S. Yamaguchi, Y. Tang, W.A. Goddard, Structures, vibrations, and force fields of dithiophosphate wear inhibitors from ab initio quantum chemistry, J. Phys. Chem. 100 (1996) 15760–15769, http://dx.doi.org/10.1021/jp960649j.

[40] N.J. Mosey, T.K. Woo, Finite temperature structure and dynamics of zinc dialkyldithiophosphate wear inhibitors: A density functional theory and ab initio molecular dynamics study, J. Phys. Chem. A 107 (2003) 5058–5070, http://dx.doi.org/10.1021/jp034085c.

[41] C. Corsini, S. Peeters, M.C. Righi, Adsorption and dissociation of ni(acac)2 on iron by ab initio calculations, J. Phys. Chem. A 124 (2020) 8005–8010, http://dx.doi.org/10.1021/acs.jpca.0c05040, pMID: 32881495.

[42] G. Losi, S. Peeters, F. Delayens, H. Vezin, S. Loehlé, B. Thiebaut, M.C. Righi, Experimental and ab initio characterization of mononuclear molybdenum dithiocarbamates in lubricant mixtures, Langmuir 37 (2021) 4836–4846, http://dx.doi.org/10.1021/acs.langmuir.1c00029, pMID: 33847121.

[43] M. Wolloch, G. Losi, M. Ferrario, M. Righi, High-throughput screening of the static friction and ideal cleavage strength of solid interfaces, Sci. Rep. 9 (2019).

[44] B. Dacre, C.H. Bovington, The adsorption and desorption of zinc di-isopropyldithiophosphate on steel, A S L E Trans. 25 (1982) 546–554, http://dx.doi.org/10.1080/05698198208983124.

[45] M. Wolloch, G. Levita, P. Restuccia, M.C. Righi, Interfacial charge density and its connection to adhesion and frictional forces, Phys. Rev. Lett. 121 (2018) 026804, http://dx.doi.org/10.1103/PhysRevLett.121.026804, URL https://link.aps.org/doi/10.1103/PhysRevLett.121.026804.

[46] R.B. Jones, R.C. Coy, The chemistry of the thermal degradation of zinc di-alkyldithiophosphate additives, A S L E Trans. 24 (1981) 91–97, http://dx.doi.org/10.1080/05698198108983001.